Colpas-Ruiz, María Angélica; Gnecco-Molina, Camilo; Pérez-Mendoza, José; Higuera-Cobos, Oscar; Jiménez-Rodríguez, Gabriel
Obtaining a hematite pigment by thermal transformation of the surface oxide of reinforcing steel bars

Universidad
Industrial de
Santander

Obtaining a hematite pigment by thermal transformation of the surface oxide of reinforcing steel bars

Obtención de un pigmento de hematita mediante la transformación térmica del óxido superficial de varillas de acero corrugado

María Angélica Colpas-Ruiz [1a], Camilo Gnecco-Molina [1b], José Pérez-Mendoza [2], Oscar Higuera-Cobos [1c], Gabriel Jiménez-Rodríguez [3]

[1] Grupo CONFORMAT, Universidad del Atlántico, Colombia. Orcid: [a] 0000-0002-5806-2533, [b] 0000-0001-7858-7524, [c] 0000-0002-4836-5215. Emails: [a] macolpas@mail.uniatlantico.edu.co, [b] cgnecco@mail.uniatlantico.edu.co, [c] oscarhiguera@mail.uniatlantico.edu.co
[2] Grupo BIOPROCESOS, Universidad del Atlántico, Colombia. Orcid: 0000-0002-3889-3495. Email: joseperez@mail.uniatlantico.edu.co
[5] Universidad del Atlántico, Colombia. Orcid: 0000-0002-4771-2959. Email: gajimro2@yahoo.com.mx

Abstract

In this investigation work, the valuation of the surface oxide waste from reinforcing steel bars through to its thermal transformation into a pigment composed mainly of hematite (α-Fe_2O_3) is reported. X-ray Fluorescence (XRF) and X-ray Diffraction (XRD) were used to determine the elemental content of the processed waste and identify the iron oxides involved in the calcination, respectively. The steelmaking waste powder is mainly composed by Fe_2O_3 (87.92 %), SiO_2 (6.13 %), CaO (1.88 %), Al_2O_3 (1.30 %) and MnO (0.77 %). The total iron content corresponds to the following iron oxides: magnetite, maghemite, wustite, lepidocrocite, hematite and goethite. The thermal treatment of the residue at temperatures of 750-850 °C and holding times of 0.5-1.50 h, showed a high conversion of precursor iron oxides into hematite, with percentages of this phase ranging between 86.4 and 94.6%. The highest hematite obtaining was achieved at a condition of 850 °C and 1.00 h.

Keywords: α-Fe_2O_3; iron oxide; pigment characterization; calcination; crystalline phases.

Resumen

En esta investigación, se reporta la valorización de la cascarilla de óxido superficial de varillas de acero al carbono mediante su transformación térmica en un pigmento compuesto principalmente por hematita (α-Fe_2O_3). Se utilizó la Fluorescencia de Rayos X (XRF) y la Difracción de Rayos X (XRD) para determinar el contenido elemental del residuo procesado e identificar los óxidos de hierro involucrados en la calcinación, respectivamente. El residuo siderúrgico en polvo se compone mayoritariamente por Fe_2O_3 (87.92 %), SiO_2 (6.13 %), CaO (1.88 %), Al_2O_3 (1.30 %) y MnO (0.77 %). El contenido total de hierro tiene principalmente el siguiente contenido en óxidos de hierro: magnetita, maghemita, wustita, lepidocrocita, hematita y goetita. El tratamiento térmico del residuo a temperaturas de 750-850 °C y tiempos de sostenimiento de 0.5-1.50 h, evidenció una alta conversión de los óxidos de hierro precursores en hematita, con porcentajes de esta fase que oscilan entre 86.4 y 94.6 %. La mayor obtención de hematita se logró a una condición de 850 °C y 1.00 h.

Palabras clave: α-Fe₂O₃; óxido de hierro; caracterización de pigmentos; calcinación; fases cristalinas.

1. Introduction

The great majority of iron-based alloys, despite of being widely used in engineering, have as their main disadvantage their low resistance to corrosion, so they must be protected by applying coatings [1]. Steel corrosion occurs mainly by two processes: i) high temperature corrosion when the metal reacts directly with the aggressive medium (O_2, etc.) and ii) electrochemical corrosion when there is a contact between the metal and electrolytes (water, saline solutions, etc.) [2]. The corrosion of structural steels is a very worrying case since this gradually induces the formation of cracks in concrete, because of the presence of corrosion products (oxides, hydroxides and oxyhydroxides) is greatly favored by the long atmospheric exposure time of the reinforcing bar during the transport and storage before installation [3-5].

During hot rolling, the steel undergoes an oxidation process which produces an oxide scale consisted of a three-layered struture: thin outer hematite (α-Fe₂O₃) layer, intermediate magnetite (Fe₃O₄) layer and thick inner layer of wustite (FeO) [6]. The composition of remnaining mill scale after steel descaling also maintains that structure [7].

In addition, the atmospheric corrosion of steel, which is a complicated electrochemical process influenced by variables such as relative humidity, temperature, chloride content, rain, etc., draws much attention due to the costs associated with the deterioration of various structures exposed to the open air [8]. The rust layer formed in carbon steels exposed to different atmospheric conditions, is mainly composed of lepidocrocite (γ-FeOOH) and goethite (α-FeOOH); there is often also maghemite (γ-Fe₂O₃) and in marine atmospheres, it is common to find magnetite (Fe₃O₄) and akaganeite (β-FeOOH) [9].

Iron and steel manufacture generate wastes of various types and properties such as rolling mill scale, mainly composed of iron oxides [10]. This mill scale has been used to obtain hematite pigments through processes that involve a heat treatment step [11-12]. Mostly methods of preparing iron (III) oxides includes a thermal transformation final stage of the iron-containing material and in some cases, thermal processes can be used as direct routes of synthesis of iron oxide particles like hematite [13]. Other steelmaking wastes similar to this scale have been used as hematite precursors, which are also used by direct heat treatment under oxidizing conditions [14]. Balbuena *et al*. [15], test a residue from ship sandblasting operations to obtain a hematite photocatalytic material, used as an additive in concrete. Della *et al*. [16] calcined steel scrap powder to obtain hematite ceramic pigments.

The existing structural relationships between the main oxides and oxyhydroxides of iron generated as products of the carbon steel corrosion may be capable of producing hematite pigments by calcination, since this is one of the most thermodynamically stable phases and the final product of many oxidation transformation processes [17], as is summarized in Figure 1. Hematite, which can vary in color from light red to dark violet depending on its particle size, is widely used as a pigment in paints, varnishes, cosmetics , rubber, paper, glass, ceramics and tiles [18-19]. In this research, we sought to use a steelmaking residue from corrugated steel rods to obtain a hematite pigment by direct heat treatment.
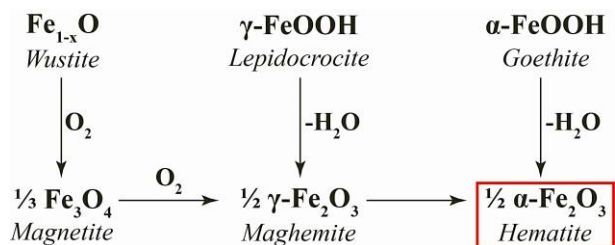

Figure 1. Structural relationships between carbon Steel corrosion products.

2. Methodology

2.1. Characterization of the hematite pigment precursor residue

The surface oxide waste from reinforcing steel bars was put through a pretreatment described below: i) 200 mesh sieving (74 μm sieve opening), ii) drying in a convection oven at 60 °C for 24 hours and iii) pulverized in a bar mill with a content of 40 %, a speed of 32 rpm for a period of 7 h/kg [14-16]. Finally, the processed residue (PR) was characterized by using several analytical techniques. The chemical composition was obtained by X-Ray Fluorescence (XRF) with a Philips® brand MagixPro PW-2440 brand Wavelength Dispersion spectrometer Fluorescence (WDXRF) [10]. The semi-quantification of the crystalline phases was determined by the software-assisted analysis of the diffractogram obtained through X-ray Diffraction (XRD) with a Panalytical® brand Empyrean 2012 model diffractometer operated with Co-K_α radiation [15,21].

In order to obtain micrographs and the elemental composition, Scanning Electron Microscopy/X-Ray Dispersive Energy Spectroscopy (SEM/EDS) was used by a Hitachi® model SU3500® scanning electron microscope with an attached Oxford Instruments® model detector X-MaxN [12,14]. The particle size distribution was determined by laser diffraction (LD) with a dry Cilas® model 990 granulometer [15,22]. The CIELAB color coordinates of the RP dispersed in coconut oil between two glass lamellae were determined by colorimetry with a DataColor® brand Check Plus model portable spectrophotometer, cofigured in a diffuse geometry with integrated/8° sphere (brightness excluded), angle from the 10° observer and light source D65 [16].

2.2. Obtaining of a pigment with high hematite content

As a preliminary heat treatment, a Rotable Central Composite Experimental Design (CCD) was used to calcinate 5 g of RP in a porcelain crucible using a Nabertherm brand LE 14/11 muffle model furnace. Two independent variables (factors) were considered in this study, the "Calcination temperature" (X_1) and the "Holding time" (X_2) with their corresponding levels summarized in Table 1, which affected the response variable, the "Hematite Percentage" (Y) [14-17].

The rotable CCD consists of: i) a 2^2 type factorial design, it is means 4 factorial runs; ii) 4 axial or star "runs" and iii) 2 runs in the center; also, each experimental combination between X_1 (750-850 °C) and X_2 (0.50-1.50 h) was replicated, for a total of 20 experimental runs [10-12]. The samples (S) of each pigment (P) obtained in the experimental design were characterized by XRD through the same analysis from a previous study [21] and by colorimetry in a similar way as was done with the PR.

Table 1. Factors and levels for the PR calcination

Factors	Levels				
X_1: Calcination temperature (°C)	850	835	800	765	750
X_2: Holding time (h)	1.50	1.35	1.00	0.65	0.50

To produce the pigment (ABP325), 2.50 kg of the residue were put in three 25 by 40 cm AISI 304 stainless steel trays on an "Industrias Protón LTDA®" brand HEMC5 model muffle furnace, under a calcination temperature of 850 °C and a holding time of 1.00 h, following the heat treatment scheme (Figure 2). The pigment turned out to

be modified by XRF, XRD, SEM/EDS, LD and colorimetry, as was done with PR. Furthermore, density and oil absorption were determined for the obtained pigment, taking into account the UNE-EN ISO 787-10: 1996 and ASTM D281-95 standards, respectively [23-24].
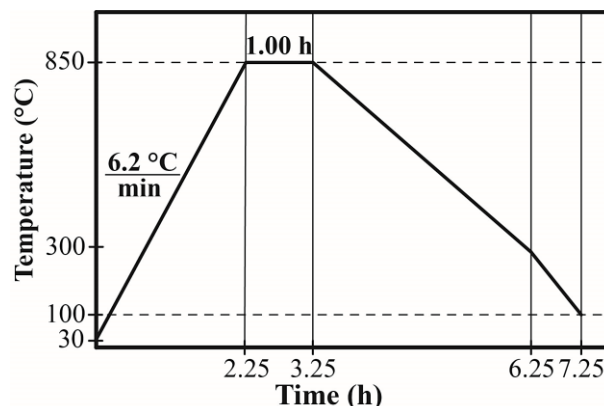

Figure 2. Heat treatment profile for the ABP325 pigment obtaining.

3. Results

3.1. Characterization of the hematite pigment precursor residue

The chemical composition of the processed residue (PR) obtained by XRF corresponds mainly to the following elements: iron (87.92 %Fe_2O_3), silicon (6.13 %SiO_2), calcium (1.88 %CaO), aluminum (1.30 %Al_2O_3) and manganese (0.77 % MnO) [10-12]. The content of the identified hematite precursor phases in the residue processed by XRD was: 26.5 %magnetite, 21.8 %maghemite, 17.0 %wustite, 14.9 %lepidocrocite and 7.3 %goetite. The presence of quartz (8.8 %) and hematite (3.7 %) was also determinated [15,21], as shown in Figure 3.

The PR particle size distribution obtained by laser diffraction was 0.3-75 µm, being the average particle size 10.10 µm. The SEM micrographs presented in Figure 4 confirmed the RP particle size and show an irregular morphology similar to that of the residue used by Sugrañez et al. [22]. Moreover, the results of the elemental analysis by EDS show that the percentages by weight of iron and oxygen were equivalent to 59.73 and 36.75 %, respectively. Likewise, the presence of silicon (2.47 %) and aluminum (1.04 %) were found. These results agree with the analyzes by chemical analysis by XRF and phase analysis by XRD.

The average color parameters values in the CIELAB coordinates for the RP dispersed in coconut oil were as follows: L^*=15.00, a^*=2.09 and b^*=5.18. These results can be compared with the CIELAB coordinates (L^*= 46.02, a^*=-0.19 and b^*=0.07) obtained for the steel scrap powder used by Della *et al*. [16]. The a^* and b^* coordinates of the PR are quite similar, but slightly higher, which may be mainly due to the contribution of the maghemite and lepidocrocyte presence. On the other hand, the PR is usually a bit darker than this steel scrap powder which has more of a metallic luster. It can be seen that the RP dispersed in coconut oil has a dark brown color (Figure 5).
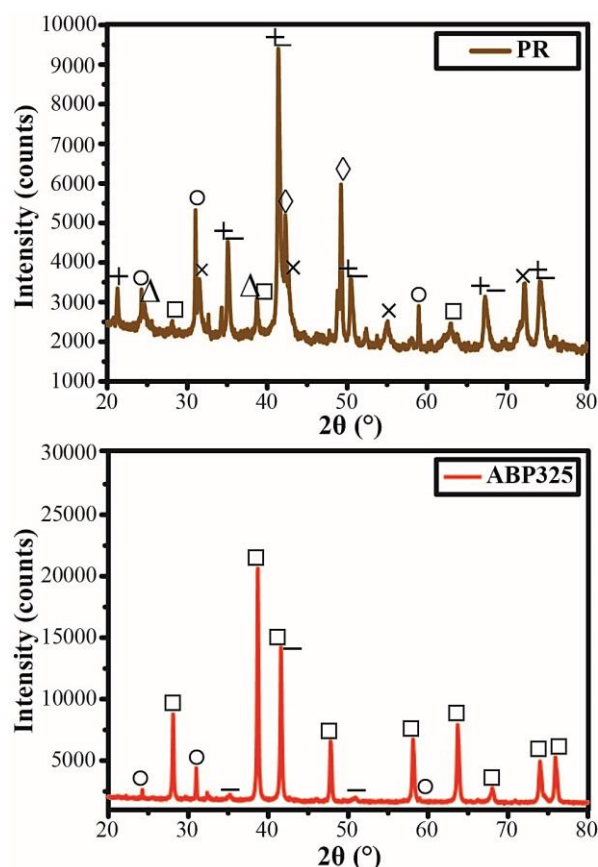

Figure 3. RP and ABP325 diffractograms. (+) Magnetite, (−) Maghemite, (×) Lepidocrocite, (◊) Wustite, (Δ) Goethite, (□) Hematite, (○) Quartz.

3.2. Characterization of synthetized hematite pigments in the experimental design

The average CIELAB color coordinates values of L^* (18.67-21.18), a^* (15.00-17.52) and b^* (9.79-15.07), indicate that the samples obtained in the experimental design dispersed in coconut oil (Table 2, Figure 5), were in the hematite commercial synthetic pigments range values for a^* from 8.40 to 22.87 and b^* from 3.23 to

35.22 reported by Cornell and Schwertmann [17]. However, the values in the range of L^* for these synthetic pigments are greater than the values obtained for all the samples of the experimental design, due to differences in the color measurement geometries used.
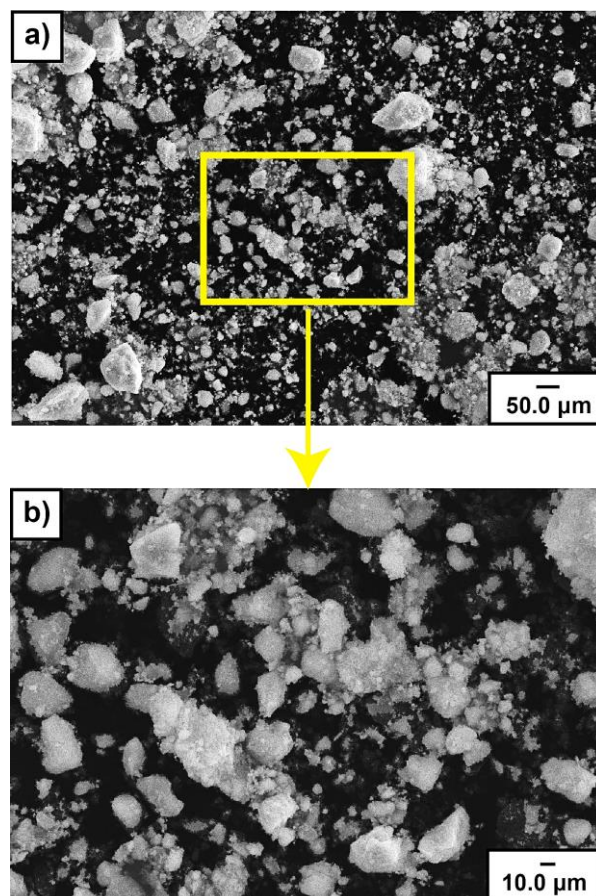

Figure 4. Processed reside (PR) SEM images. a) 1000 X. b) 3000 X

The a^* and b^* values were affected mainly by the calcination temperature. For example, for a calcination temperature of 850 °C with a holding time of 1.00 h, a^* and b^* values are lower than those obtained at 800 ° C and 750 °C with the same holding time. For this reason, pigments obtained at higher temperatures are often more bluish (Table 2, Figure 5).

The behavior described above coincides with the obtained hematite pigments trend from steel scrap powder calcination proved by Della *et al*. [16]. The pigments are also more bluish as the holding time increases (0.50, 1.00 and 1.50 h) for the same calcination temperature (800 °C). Furthermore, this trend of obtaining hematite pigments with a distinctive blue hue is the product of the influence of a relatively thick particle size, which is in accord with Schaufler *et al*. [25].
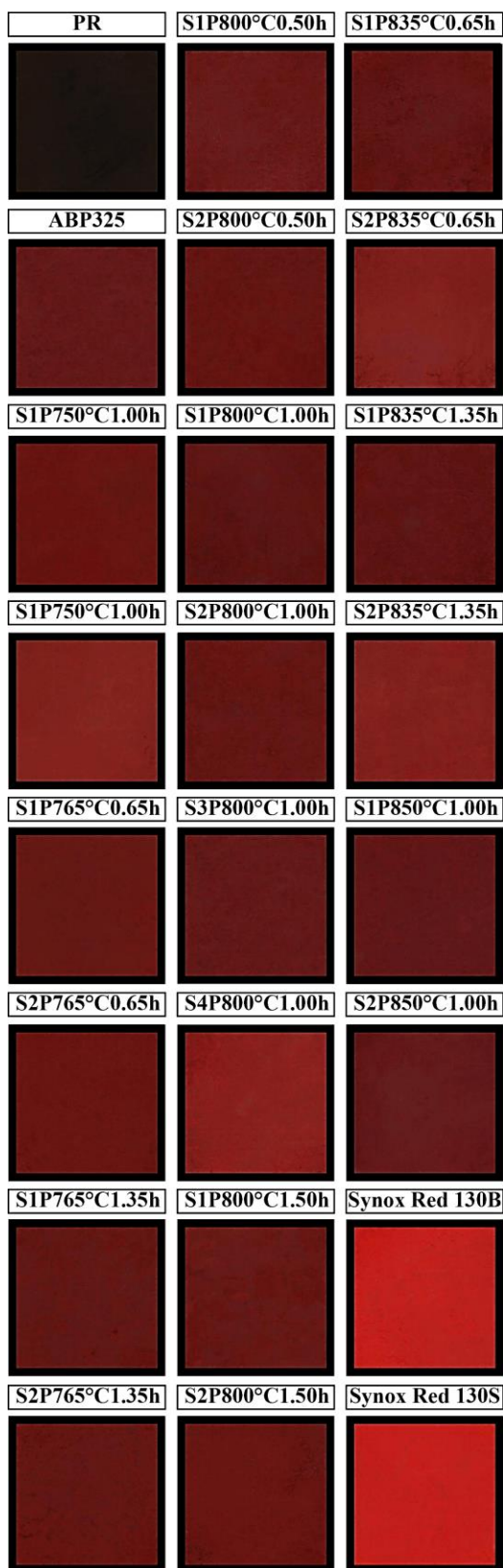
Figure 5. PR and obtained pigments dispersed in coconut oil.

Table 2. CIELAB coordinates of the synthesized pigments in the experimental design

Sample	L*	a*	b*
S1P750°C1.00h	19.08	17.52	14.63
S2P750°C1.00h	20.04	17.21	15.07
S1P765°C0.65h	21.09	16.09	12.46
S2P765°C0.65h	21.18	17.25	13.29
S1P765°C1.35h	19.66	16.06	12.94
S2P765°C1.35h	19.77	16.07	11.84
S1P800°C0.50h	19.92	15.63	10.64
S2P800°C0.50h	19.32	15.18	10.27
S1P800°C1.00h	19.21	15.91	12.25
S2P800°C1.00h	18.67	16.26	11.58
S3P800°C1.00h	19.39	16.64	12.18
S4P800°C1.00h	18.77	17.03	12.83
S1P800°C1.50h	20.02	15.23	11.07
S2P800°C1.50h	19.99	15.00	9.79
S1P835°C0.65h	19.36	17.09	12.47
S2P835°C0.65h	18.72	17.66	13.29
S1P835°C1.35h	19.05	16.21	11.54
S2P835°C1.35h	19.02	16.59	11.53
S1P850°C1.00h	18.28	15.91	10.93
S2P850°C1.00h	19.08	16.50	11.18

Table 3. Crystalline phases of the obtained hematite pigments in the calcination experimental design

Sample	Crystalline phases		
	% α-Fe$_2$O$_3$	% γ-Fe$_2$O$_3$	% SiO$_2$
S1P750°C1.00h	87.0	6.4	6.6
S2P750°C1.00h	86.4	8.0	5.6
S1P765°C0.65h	87.3	7.0	5.7
S2P765°C0.65h	88.3	5.3	6.4
S1P765°C1.35h	88.8	4.5	6.7
S2P765°C1.35h	87.5	5.6	6.9
S1P800°C0.50h	89.2	5.4	5.4
S2P800°C0.50h	90.7	3.4	5.9
S1P800°C1.00h	90.6	2.2	7.2
S2P800°C1.00h	90.1	3.6	6.3
S3P800°C1.00h	92.9	2.3	4.8
S4P800°C1.00h	90.4	4.0	5.6
S1P800°C1.50h	91.5	1.5	7.0
S2P800°C1.50h	92.4	1.9	5.7
S1P835°C0.65h	94.3	0.2	5.5
S2P835°C0.65h	93.3	0.7	6.0
S1P835°C1.35h	94.5	0.2	5.4
S2P835°C1.35h	94.5	0.3	5.3
S1P850°C1.00h	**94.5**	**0.1**	**5.4**
S2P850°C1.00h	**94.6**	**0.0**	**5.4**

Table 3 shows the percentages of the crystalline phases derived from the Rietveld refinement of the pigments diffractograms obtained by XRD, after calcination temperature and the holding time in the heat treatment are varied. The hematite content variations of 3.7 % up to an interval from 86.4 to 94.6 % indicate that calcination promoted the conversion of the precursor phases in hematite. The samples calcined at 750 °C for 1.00 h has the lowest percentages of hematite. In contrast, the precursors were converted almost entirely in hematite after heating the residue up 850 °C for 1.00 h, thus obtaining the highest percentage of hematite [21].

3.3. Characterization of the obtained hematite pigment (ABP 325)

The results of semi-quantification analysis obtained by XRF determined that the pigment produced (ABP325) was mainly composed of iron (85.79 %Fe_2O_3), silicon (6.45 %SiO_2), calcium (2.16 %CaO), sulfur (1.55 %SO_3) and aluminum (1.46 %Al_2O_3). Small amounts of other elements were also observed: Mn, Na, K, Mg, P, Cl, Ti, Cr, Cu, Zn, Ni, Pb and Mo. The elements identified in ABP325 coincide with those identified in the hematite ceramic pigments synthesized by Della et al. [16].

From the semi-quantitative analysis of the diffractogram obtained by XRD for ABP325, a composition of 91.4% hematite, 3.1% maghemite and 5.5% quartz were determined, which demonstrate a high conversion of the precursor phases that constituted around 88% of the PR (Figure 3). On the other hand, the pigment has a morphology characterized by an irregular shape and size particle (Figure 6). This is complemented by the particle size distribution results obtained through LD, with values mainly between 0.3 and 45 µm (average particle size of 14.57 µm), which is in accordance with the specifications of ASTM D185-07 (2019) to be used as a pigment [26].

Elemental analysis by EDS exhibits iron and oxygen concentrations equivalent to 55.69 % and 40.71 %, respectively. The presence of silicon (2.70%) and aluminum (0.91%) is also observed. These results confirms a high amount of iron and oxygen estimated at 96.40 % of the total sample analyzed, being the remaining 3.60 % attributed to silicon and aluminum impurities. These results are quite similar to the elemental chemical analysis by EDS of the PR, since there was only a transformation of the different crystalline phases of precursor iron oxides into hematite and maghemite.

The density values for two replicas of the obtained pigment PAB325 (3.84 and 3.85 g/ml) are close to the lower value of the specific gravity range (4.0-5.0),

reported for synthetic red iron oxide pigments with a purity of ~85 %Fe_2O_3 [27] . The density of the pigment obtained was influenced by irregular shape, relatively high particle size and low expected surface area, as has been indicated by Oyarzún [28]. The oil absorption values for two replicas of obtained pigment (ABP325) were 15.36 and 16.34 g/100 g of pigment, respectively. These values are consistent with the oil absorption range for hematite pigments (15-30) and are highly dependent on the large particle size (14.57 µm) of ABP325 and even on the nature of the obtained product [29-30].
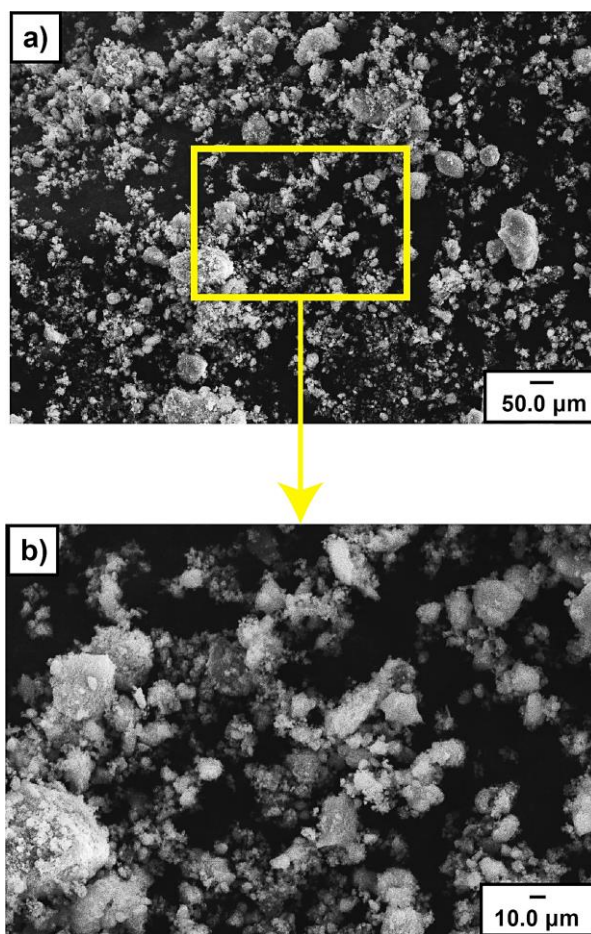

Figure 6. Obtained Pigment (APB325) SEM Images. a) 1000 X. b) 3000X

Oil absorption values generally depend on the pigment production method [11], since they get bigger with increasing density [31] or decreasing particle size [32]. The high purity pigment (95.3 %Fe_2O_3) synthesized from mill scale by Quddus et al. [12], had an oil absorption value of 29.99 g/100 g of pigment compared to a value of 28 g/100 g of pigment for a recognized commercial pigment (Bayferrox® 110) and 19.77 g/100 g of pigment for another cheaper commercial pigment.

The CIELAB coordinates of ABP325 dispersed in coconut oil (Figure 5) are: L^*=20.3; a^*=15.7 and b^*=10.8. These results differ with the obtained results for the samples of the experimental design synthesized to the same calcination condition (850 ° C and 1.00 h), because of the large-scale change did not achieve the same chemical purity and phase composition [32]. The bluish-red color pigment ABP325 coincides with a^* (13.3 and 21.1) and b^* (5.0 and 8.0) values of some high purity hematite pigments sythetized through magnetite calcination by Schaufler et al. [25]. Red hematite can be converted to purple hematite by modifying its particle size sufficiently, as is explained by Cornell and Schwertmann [17], due to there is evidence that heating hematite to temperatures above 800 °C causes a color change towards purple, due to the transformation of associations of small hematite crystals into oriented aggregates.

Synox® commercial synthetic hematite pigments dispersed in coconut oil can be used as a reference for the pigment obtained (Figure 5), which has the following color coordinates: Red 130B (L^*=23.83, a^*=29.09 and b^*=24.66) and Red 130S (L^*=23.30, a^*=28.94 and b^*=23.73). These commercial reference pigments has much higher values of the a^* and b^* coordinate which indicates a yellowish-red color very different from the bluish tone of ABP325. This apparent discrepancy is mainly due to the much smaller particle size of these commercial pigments [25-26].

4. Conclusiones

Crystalline phases characterization by XRD of the processed residue "PR" confirmed the presence of all the corrosion products reported on reinforcing steel bars by Zitrou et al. [3]. Furthermore, mainly iron oxides coincide with the atmospheric corrosion products identified in the oxide scale of a carbon steel structure characterized in a very similar way by Velázquez and Jaramillo [33].

The nature of surface oxide waste from reinforcing carbon steel bars allowed its use as hematite precursor through direct thermal treatment achieved with simplicity after the correct choice of the experimental conditions involved in the calcination [13]. The obtained hematite showed properties that qualify it as a pigment [27], therefore it can be implemented in various applications [19], such as in the field of paints [29].

Suggestions

It is considered interesting to investigate other aspects related to the heat treatment and management of the recovered iron and steel waste, as well as the implementation of the obtained hematite pigments in various fields. Likewise, the grinding time of similar steelmaking residues will be increased to produce a hematite pigment precursor, with a more micronized particle size, since this will has greatly influence in the final properties of target products, it is means the pigment will have values of density, surface area, oil absorption, colorimetric coordinates, etc., closer to the other commercial hematite pigments.

Acknowledgements

References

[1] D. E. J. Talbot, J.D.R. Talbot, "Corrosion of Iron and Steels," in *Corrosion Science and* Technology, 3rd ed. Boca Raton, US: CRC press, 2018, pp. 195-214.

[2] M. Morcillo, B. Chico, "Conceptos básicos sobre corrosión atmosférica," in *La corrosión atmosférica del acero al carbono en ambientes costeros*. Madrid: Editorial Consejo Superior de Investigaciones Científicas (CSIC), 2018, ch. 2, pp. 32-59.

[3] D. de la Fuente, J. Alcántara, B. Chico, I. Díaz, J.A. Jiménez, M. Morcillo, "Characterisation of rust surfaces formed on mild steel exposed to marine atmospheres using XRD and SEM/Micro-Raman techniques," *Corros. Sci.*, vol. 110, pp. 253–264, 2016, doi: 10.1016/j.corsci.2016.04.034

[4] Y. Zhao, H. Ren, H. Dai, W. Jin., "Composition and expansion coefficient of rust based on X-ray diffraction and thermal analysis," *Corr. Sci.,* vol. 53, no. 5, pp. 1646–1658, 2011, doi: 10.1016/j.corsci.2011.01.007

[5] E. Zitrou, J. Nikolaou, P. E. Tsakiridis, G. D. Papadimitriou, "Atmospheric corrosion of steel reinforcing bars produced by various manufacturing processes," *Rev. Constr. Build. Mat.*, vol. 21, no. 6, pp. 1161-1169, 2007, doi: 10.1016/j.conbuildmat.2006.06.004

[6] R. Chen, W. Y. D. Yuen, "A study of the scale structure of hot-rolled steel strip by simulated coiling and cooling," *Oxid. Met.*, vol. 53, no. 5-6, pp. 539-560, 2000, doi: 10.1023/A:1004637127231.

[7] R. Bhattacharya, G. Jha, S. Kundu, R. Shankar, N. Gope, "Influence of cooling rate on the structure and formation of oxide scale in low carbon steel wire rods during hot rolling," *Surf. Coat. Tech.*, vol. 201, no. 3-4, pp. 526-532, Oct. 2005, doi: 10.1 016/j.surfcoat.2005.12.014

[8] P. Schweitzer, "Atmospheric Corrosion," in *Fundamentals of metallic corrosion: atmospheric and media corrosion of metals* (Corrosion Engineering Handbook, 2nd ed.). Boca Raton, US: CRC press, 2006, ch. 2, pp. 39-66.

[9] J.G. Castaño, C.A. Botero, A.H. Restrepo, E.A. Agudelo, E. Correa, F. Echeverría, "Atmospheric corrosion of carbon steel in Colombia," *Corr. Sci.*, vol. 52, no. 1, pp. 216-223, 2010, doi: 10.1016/j.corsci.2009.09.006

[10] H. Ovčačíková *et al*., "Possibilities of recycling of oiled scale for preparation of pigments," *Rev. Acta Metallurgica Slovaca-Conference*, vol. 4, pp. 90-97, 2014, doi: 10.12776/amsc.v4.217

[11] P. Zevallos, D. Flores, "Síntesis y caracterización de pigmentos de hematita obtenidos a partir de cascarilla de laminación," B.Sc. Thesis. Fac. Ing. Proc., Univ. Nac. San Agustín, 2015. Available: http://repositorio.unsa.edu.pe/bitstream/handle/UNSA/1 94/B2-M-18321.pdf?sequence=1&isAllowed=y.

[12] M. S. Quddus *et al*., "Synthesis and Characterization of Pigment Grade Red Iron Oxide from Mill Scale," *IRJPAC*, vol. 16, no. 4, pp. 1-9, 2018, doi: 10.9734/IRJPAC/2018/42935

[13] R. Zboril, M. Mashlan, D. Petridis, "Iron (III) oxides from thermal processes synthesis, structural and magnetic properties, Mössbauer spectroscopy characterization, and applications," *Chem. Mater.*, vol. 14, no. 3, pp. 969-982, 2002, doi: 10.1021/cm0111074

[14] A. C. da Silva *et al.*, "Converting Fe-rich Magnetic Wastes into Active Photocatalysts for Environmental Remediation Processes," *J. Photoch. Photobio. A*, vol. 335, pp. 259-267, 2017, doi: 10.1016/j.jphotoche.2016.11.025

[15] J. Balbuena *et al*., "Preparation of self-cleaning and de-poluting building materials through the valorization of industrial wastes," in 33rd *Cement and Concrete Science Conf.*, Portsmouth, UK, 2013, pp. 189-194.

[16] V. Della, J. A. Junkes, O. R. K. Montedo, A. P. N. Oliviera, C. R. Rambo, D. Hotza, "Synthesis of hematite from steel scrap to produce ceramic pigments," *Rev. Am. Ceram. Soc. Bull*, vol. 86, no. 5, pp. 9101-9108, 2007.

[17] R. M. Cornell , U. Schwertmann, "Transformations," in *The Iron Oxides: Structure, Properties, Reactions, Occurrences and Uses*, 2nd ed. Weinheim, Germany: Wiley-VCH, 2003, ch. 14, pp. 365-409.

[18] J.G. Castaño, C. Arroyave, "La funcionalidad de los óxidos de hierro," *Rev. Metal. Madrid*, vol. 34, no. 3, 1998. [Online]. Available: http://revistademetalurgia.revistas.csic.es/index.php/revi stademetalurgia/article/view/794/805

[19] G. Buxbaum, G. Pfaff, "Colored Pigments," in *Industrial Inorganic Pigments*, 3rd ed. Weinheim, Germany: Wiley-VCH, 2005, ch. 3, pp. 99-162.

[20] A. M. Olmedo, "Estudio de películas de óxidos de hierro crecidas y depositadas en diversos ambientes," Ph.D. Dissertation, Fac. Cien. Exac. Nat. Univ. Buenos Aires, Argentina, 1990. Available: http://hdl.handle.net/ 20.500.12110/tesis_n2320_Olmedo.

[21] M. A. Colpas, C. Gnecco, J.A. Pérez, O. F. Higuera, G. A. Jiménez. "Synthesis of an Anticorrosive Pigment by Thermal Treatment of Iron Oxides from Steel Industry Wastes," *Rev. Fac. Ing.*, vol. 28, no. 52, pp. 43-58, 2019, doi: 10.19053/01211129.v28.n52.2019.9653

[22] R. Sugrañez *et al*., "Preparation of sustainable photocatalytic materials through the valorization of industrial wastes," *Rev. ChemSusChem*, vol. 6, no. 12, pp. 2340-2347, 2013, doi: 10.1002/cssc.201300449

[23] Métodos generales de ensayo para pigmentos y extensores. Parte 10: Determinación de la densidad. Método del picnómetro, UNE-EN ISO 787-10, 1996.

[24] Standard Test Method for Oil Absorption of Pigments by Spatula Rub-out, ASTM D281-95(2016), 2016, doi: 10.1520/D0281-12R16

[25] L. Schaufler *et al*., "Seeing Red: Colour space and potential in hematites," *Rev. European Coatings Journal*, no. 3, pp. 132-137, 2019.

[26] *Standard Test Methods for Coarse Particles in Pigments*, ASTM D185-07, 2019.

[27] N. Veeramani, "Inorganic Pigments-II", *Paintindia Mag.*, vol. 66, no. 6, pp. 86-90, Jun. 2016.

[28] J. Oyarzún, "Physical characterisation of pigments," in *Pigment Procesing: Physico-Chemical Principles*, 2nd ed. Hannover, Germany: Vincentz Network, 2015, ch. 1, pp. 13-51.

 [29] A. Ribadeneira, "Protección anticorrosiva del acero mediante el uso de pinturas alquídicas con pigmentos de óxido de hierro en atmósferas urbana y subtropical", B.Sc. Thesis. Fac. Prof. Ing. Agro., Univ. Escuela Politécnica Nacional, 2008. Available: https://bibdigital.epn.edu.ec/handle/15000/1686

[30] J. Calvo, "Pigmentos y Cargas," in *Pinturas y recubrimientos: introducción a su tecnología*. Madrid, España: Ediciones Díaz de Santos, 2009, ch. 2, pp. 9-29.

[31] F. Jones, M. Nichols, S. Pappas, "Pigment Dispersion," in *Organic Coatings: Science and Technology*, 4th ed, Hoboken, US: John Wiley & Sons, 2017, ch. 21, pp. 307-322.

[32] D. Mannari and C. Patel. "Pigments," in *Understanding Coatings Raw Materials*. Hannover, Germany: Vincentz Network, 2015, ch. 3, pp. 139-208.

[33] A. A. Velásquez, D. Jaramillo Raquejo, "Characterization of the corrosion products of one of the pedestrian paths of the bridge "Punto Cero" in the city of Medellin, Colombia," *J. Phys.: Conf. Ser*., vol. 1247, Paper. 012022, Jun. 2019, pp. 1-10. doi: 10.1088/1742-6596/1247/1/012022